HiSST: 3rd International Conference on High-Speed Vehicle Science Technology
14 -19 April 2024, Busan, Korea

The Scramjet Hypersonic Experimental Vehicle

S. Di Benedetto[1], M. Marini[1], P. Roncioni[1], A. Vitale[1], P. Vernillo[1], G. Di Lorenzo[1], R. Scigliano[1], S. Cardone[2], M. Albano[3], R. Bertacin[3]

Abstract

The research and experimentation for hypersonic flight, aimed at creating and testing the enabling technologies for future high-speed systems, is one of the main research topics Europe has been engaging for over 20 years, mainly with the projects dedicated to hypersonic flight for passenger transport (HEXAFLY [1], HEXAFLY-INT [2], LAPCAT I&II [3], ATLLAS I&II [4], FAST20XX [5], STRATOFLY [6]).
In this frame the Italian Aerospace Research Centre (CIRA), by means of the national program PRORA, and the Italian Space Agency (ASI) funded a project aimed at designing a propelled hypersonic demonstrator, the Scramjet Hypersonic Experimental Vehicle, and its flight experimental mission.
The paper presents the baseline air-launched mission scenario that foresees the use of a carrier aircraft and a launch vehicle propelled by a booster to drive the scramjet demonstrator at the defined experimental window, and the first results and evaluations on the demonstrator configuration.
A first assumption on the scale of the demonstrator has been done, and its materials layout, its avionics, airframe and the components of propulsive subsystems, including the on-board fuel tanks (hydrogen) for the scramjet engine properly sized.
Massive CFD simulations along the flight trajectory have allowed the verification of the aero-propulsive balance and the definition of aerothermal loads and aerodynamic coefficients which have been used for the thermal analysis and the flight mechanics analysis and trajectory calculation, respectively.

Keywords: *Hypersonics, scramjet, flight test, air-launching, multidisciplinary design*

Nomenclature

AoA – Angle of Attack
ACU - Actuators Control Unit
AEDB – Aerodynamic Database
ASI – Italian Space Agency
CD - Drag Coefficient
CFD – Computational Fluid Dynamics
CIRA – Italian Aerospace Research Center
CL –Lift Coefficient
CoG – Centre of Gravity
COTS - Off-the-Shelf component
DAQ – Data Acquisition system
EC – European Commission
EGSE – Electrical Ground Support Equipment
EMC - Electromagnetic Compatibility
FCC - Flight Control Computer
GN&C – Guidance Navigation and Control
IFMS - In-flight measurement system
L/D – Aerodynamic Efficiency
LV – Launch Vehicle
PDR – Preliminary Design Review
POW - Power Management System
PYRO - Pyro Control
RF – Radio Frequency
SHEV – Scramjet Hypersonic Experimental Vehicle
S/S – Subsystem
SW - Software
TT&C - Telemetry and Telecommand

[1] *CIRA Italian Aerospace Research Centre, 81043 Capua, Italy, s.dibenedetto@cira.it*
[2] *Tecnosistem, 80133 Napoli Italy, scardone@tecnosistemspa.it*
[3] *ASI, Agenzia Spaziale Italiana, 00133 Rome, Italy, marta.albano@asi.it*

1. Introduction

The research and experimentation for hypersonic flight, aimed at creating and testing the enabling technologies for future high-speed systems, is one of the main research topics on which CIRA has been engaged for over 15 years, mainly with the participation on the various EC projects dedicated to hypersonic flight for passenger transport (HEXAFLY [1], HEXAFLY-INT [2], LAPCAT I&II [3], ATLLAS I&II [4], FAST20XX [5], STRATOFLY [6]), but also with military and civil national projects.
In 2021 CIRA, thanks to the "SPACE-IPERSONICA-TEC" project, funded by the national program PRORA, and taking advantage from its strong involvement in the European projects just mentioned, and in particular in HEXAFLY-INT (flight test of an unpropelled vehicle for hypersonic flight), and previously in HEXAFLY, posed the challenge of designing a scramjet hypersonic demonstrator for a future test in-flight.
In 2022, as the project was of high interest also of the Italian Space Agency, the two national entities decided to co-fund the research activities by a dedicated agreement "Research and Development of a hypersonic demonstrator", which has the aim at completing the project Preliminary Design Review by 2025.
The main project objectives have been defined considering also the international scenario of propelled hypersonic aircraft, analysed from the sixties to today, ranging from U.S. experimental vehicles (X-15A, X-43A, X-51A), which have actually flown, to experimental vehicles in national or international cooperation initiatives in recent years, such as the Brazilian 14-X, the Franco-Russian project LEA and the project funded by the European Commission HEXAFLY. The research criterion was to select only propelled hypersonic vehicle demonstrators designed to create and test the enabling technologies for future hypersonic civil transport systems, thus leading to the following system and mission high-level objectives:

- Aircraft class: length 3÷8 m, mass 600÷2000 kg
- Hypersonic flight at Mach=6÷8, constant altitude 27÷32 km, stable and trimmed
- Aero-propulsive balance with an aerodynamic efficiency L/D=3÷4
- Scramjet propulsion system with hydrogen as fuel, running steadily for at least 10 seconds.

This paper deals with the activities performed at system level for the system and mission definition.
The approach defined is based on the tight interaction between subsystems up to the completion of system and mission design, as described in the flow chart below (see Fig 1). The process is coordinated by the system, which represents the design authority, to fulfil the mission and system requirements defined from the mission objectives.
The flow chart clarifies how, in the multidisciplinary approach, each discipline interacts with the other ones and with the system itself, and which parameters are being exchanged.

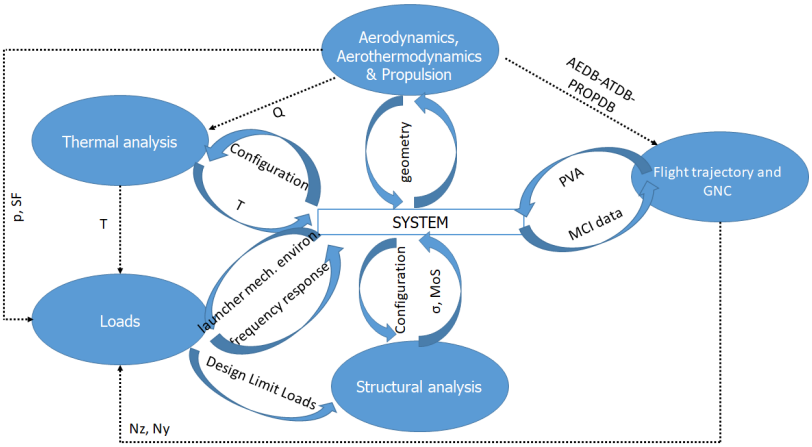

Fig 1. Multidisciplinary interactions and interdependencies within the different disciplines

2. Mission Scenario

The preliminary mission concept envisages an air-launched solution with a carrier (stage I) capable of releasing the payload, composed by the hypersonic demonstrator and an aerodynamically controlled launch vehicle equipped with a booster, at a target point in terms of speed and altitude, preliminary assumed as (Table 1):

Table 1. Release conditions of the payload from the carrier aircraft

Altitude	13.5-15 km
Mach number	0.6

From here the launch vehicle accelerates until it reaches the foreseen trajectory target point (experimental window) where the hypersonic propelled demonstrator is separated from the launch vehicle and the scramjet starts working, as graphically described in Fig 2.
Note that it is assumed that the carrier aircraft returns back and lands at the airport, whilst both the launch vehicle and the hypersonic propelled demonstrator are disposable vehicles, thus they are not recovered.

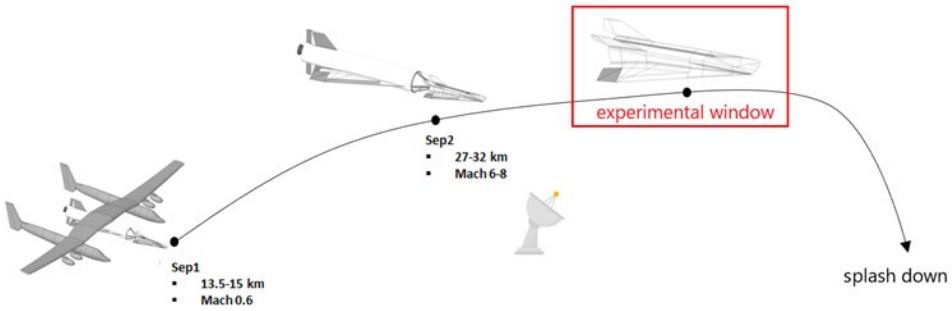

Fig 2. Graphical representation of the experimental mission scenario

The preliminary design of the launch vehicle is shown in Fig 3.

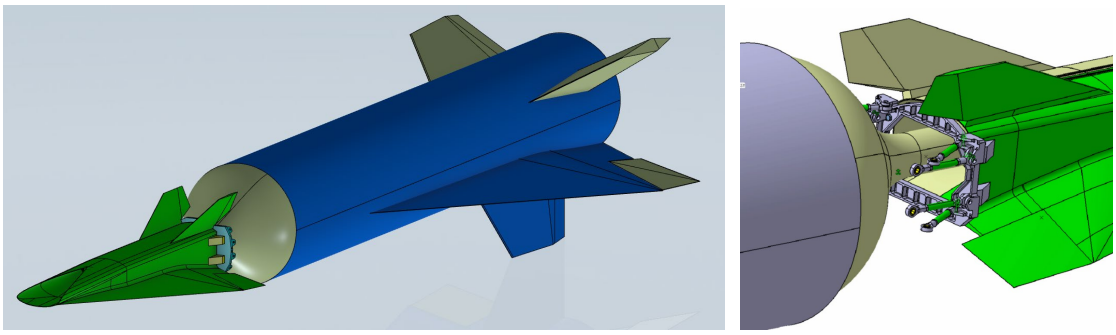

Fig 3. Details of the launch vehicle assembled with the SHEV

2.1. Launch Vehicle Booster design

From the execution of the mission shown in Fig 2, the ORION 50 ST booster form Northrop Grumman was identified on the base of the following main parameters:

- thrust (ΔV) that the propulsion system must be able to provide to complete the mission;
- average acceleration which the booster and the hypersonic demonstrator are subjected to;
- firing time;
- total weight;
- maximum available dimension to install the booster;
- the ratio between the expelled mass and the inert mass.

This selection allows us to have a relatively high margin on the mission's ΔV, so fixing the diameter makes it possible to calculate how much the length and therefore the total weight of the booster must decrease to optimize it for the mission at hand.
In order to design a booster capable of meeting the needs of missions for the launch vehicle, the following phases have been developed:

1. Final mass sizing of the reduced Orion 50 ST booster (grain, case and nozzle);

To obtain a plausible estimate with acceptable design margins, the "effective" mass of the booster was considered, taking into account the required propellant weight and deducting the "invariant" inert masses with respect to the mission.

2. Final concept of the nozzle (length and divergent angle, known the exit section diameter);

To make a plausible estimate of the nozzle weight, its shape was determined based on the data defined in the Orion 50 ST datasheet.

3. Combustion chemistry and nozzle exit conditions;

The thermodynamic conditions of the nozzle exit were thus determined, to be used for the aerodynamic CFD simulations.

4. Assumptions on grain consumption (radial), effect on the Centre of Gravity;

Given the thrust profile, it was assumed that the grain was at the "central port", a geometry that allows for a nearly constant profile (except for the initial part of ignition). This also allowed for a fairly precise determination of the location of the various CoGs of the booster system, and consequently to evaluate the booster global CoG axial displacement following propellant consumption.

5. Adaptation of the thrust profile to the new motor/firing time;

Once the required propellant mass to complete the mission was identified, assuming the grain was constant-section and central port (as in the previous point), the "effective" thrust exerted by the booster due to its length variation was determined.

Fig 4-left shows the booster in its initial configuration. In the plot on the right, the motor thrust trend is also shown. Based on the reduction in propellant necessary for the mission, and consequently the reduction in length and in internal surface area of the grain gate, a reduction in the thrust equal to 18% has been estimated. Indeed, assuming the geometry of the grain with a central port, we can scale the thrust proportionally to the variation in length because the burning rate (which depends only on the propellant and the boundary conditions) is constant. The thrust will depend only on the propellant flow rate which in turn depends on the combustion surface which, since the geometry is axially constant, will depend only on the length. Thus, the thrust depends linearly on the length of the propellant. This value is of course preliminary and will be calculated in detail only once the "effective" geometry of the reduced grain will be defined.

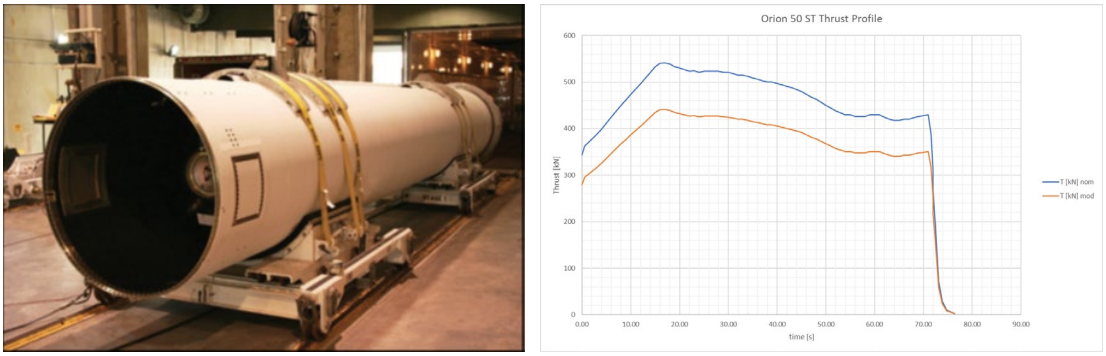

Fig 4. Standard configuration image of ORION 50 ST (left); thrust curve comparison between nominal and modified (right)

3. The Scramjet Hypersonic Experimental Vehicle

3.1. Configuration of the flight demonstrator

The configuration of the Scramjet Hypersonic Experimental Vehicle (SHEV) is based on the concept of "waverider", i.e., a hypersonic vehicle with high aerodynamic efficiency in supersonic regime obtained

through the exploitation of the shock waves that form on the load-bearing surfaces, a phenomenon known as "compression lift".
The demonstrator must also include a scramjet air-breathing propulsion system.
For this concept, in particular, the configuration studied in the EU-FP7 HEXAFLY project [1] was considered as starting point and then modified to meet the specific project objectives, thus leading to the configuration depicted in Fig 5, with the following main features:

- L=4.5 m, W=1.76 m
- Mass 1000÷1200 kg

The demonstrator is equipped with its own avionic and in-flight measurement system, whose definition is ongoing. The main avionic subsystems are: Power Management System, Flight Control Computer (FCC), In-flight measurement system (IFMS), servo-actuator and Pyro Control (ACU, PYRO), Telemetry and Telecommand (TT&C), Scramjet Control Unit.

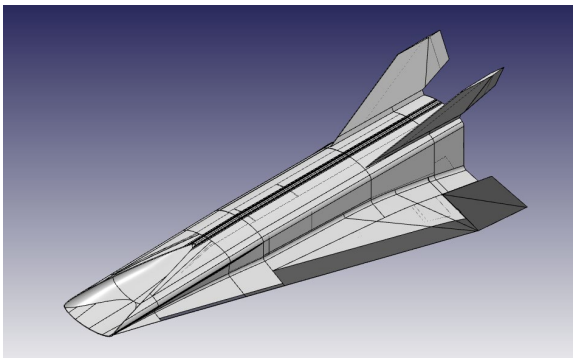

Fig 5. SHEV external configuration

The complexity of the structure is strictly related to the fuel tanks allocation and the presence of the integrated combustion chamber. These two main elements, that obviously reduce the room available inside the vehicle, together with the high temperature reached during the mission, make the design very challenging. Based on the main requirements and the preliminary information, the structural configuration has been defined by means of a build-up approach. The different structural elements, mainly frame panels and spars assembled, composed of different materials as indicated in the following, are shown in Fig 6.
The structure is mainly composed by milling frames, upper beams and panels. The assembly of fuselage structure is realized by joining upper beams, upper frames and lower frame with fixed bolts, the upper panels are joined to the frames and upper beams by removable bolts in order to allow the access inside of the fuselage for the installation of internal equipment (see Fig 7).

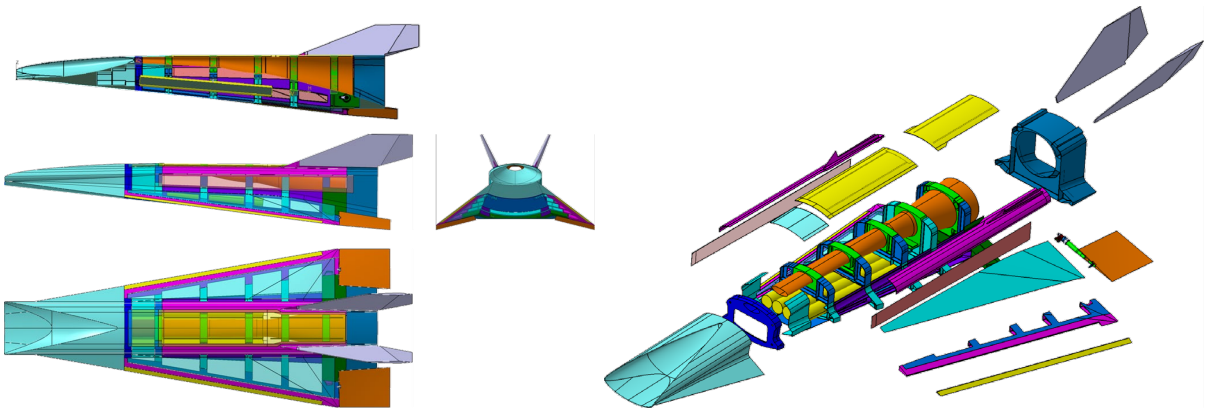

Fig 6. SHEV main structural elements

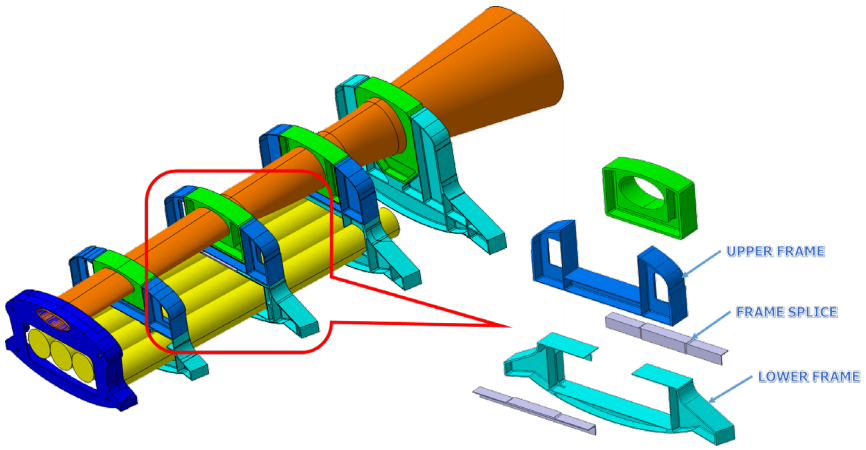

Fig 7. SHEV Structural Configuration

The preliminary materials layout has been defined on the base of several transient thermal analyses where different materials and layouts have been analyzed**.** The main criticalities have been highlighted and overcome either by changing material or by changing the material layout. This iterative approach has led to the optimal thermal distribution [7].
In particular, for the set of structural external parts where the use of high temperature material is needed ("hot structure"), ISiComp® [8] ceramic material has been applied (see Fig 8-left): flaps, wing leading edges, intake, external part of propulsive duct. The remaining external parts belong to the cold structure subsystem (Fig 8-right).
ISiComp® is the material chosen also for the combustion chamber and the entire propulsive path, with exception of the struts for the injection of fuel where higher temperatures are expected and the use of molybdenum is recommended [7].

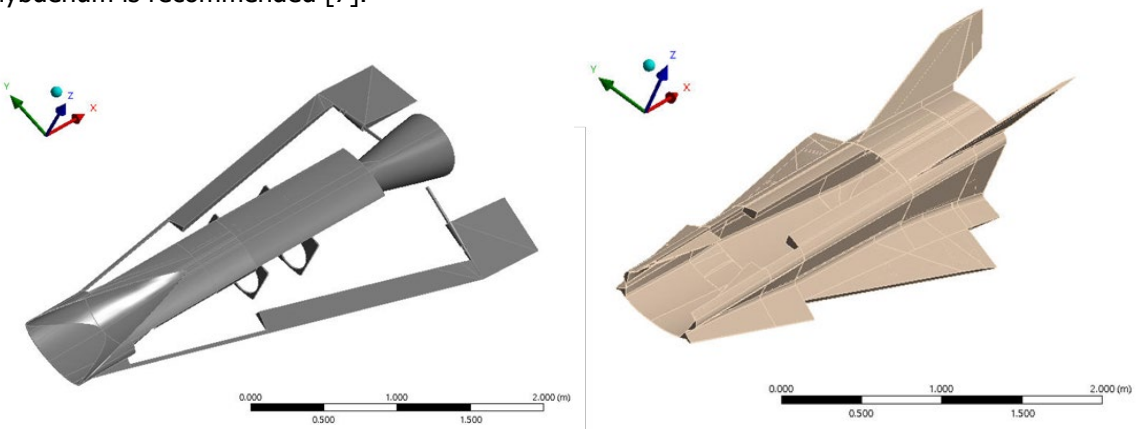

Fig 8. SHEV external structure material layout**:** ISiComp® components (left), Titanium components (right)

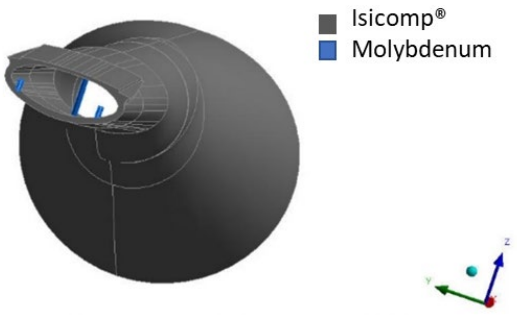

Fig 9. SHEV Molybdenum struts in the combustion chamber

3.2. Avionic System Design

The Avionic system of the vehicle mainly aims to identify the functions to be exploited by the vehicle along the mission phases.
The current architecture is based on the typical main S/S of a Space Vehicle, e.g. Flight Control System (FCC), Power management system (POW), Telemetry & Telecommands system (TT&C), In Flight Measurement System (IFMS), Actuators Control Unit (ACU).

The **Power management system** main functions are:

- To retrieve power from electric energy sources, e.g. CoTS Li-Ion batteries, and to perform:
  - Voltage Level adaptation and stabilization;
  - Filtering in compliance with EMC specs and power protection;
  - Power dispatching to the single units;
  - Tell-backing statuses of power feeding the single units;
- To power feed the High Level-Power-Demanding Units (e.g. Actuators, RF Transmitters, ...);
- To power feed the Normal Level-Power-Demanding Units (e.g. Computer, DAQ, ...);
- To power feed the Impulsive-Demanding Units (e.g. pyro for separations);
- To provide with physical power links to the avionic units and EGSE.

The **Flight Control System** aims:

- To provide with a physical platform (On-Board Computer) for running the SW for :
  - State Machine for managing all the phases of the unmanned vehicle (under Launch Vehicle control, under GN&C control, ...);
  - GN&C Algorithms for the flight phases under GN&C control;
  - Data Acquisition, Conversion, Sharing; physical I/F data conversion and management;
  - Management of data from/to TM/TC;
  - Time and synchronization management;
- To control the Actuators and actuation surfaces of the vehicle through the GN&C SW;
- To control the Vehicle scramjet propulsion and the Booster phase;
- To acquire and exploit the GPS and IMU data for GN&C purposes;
- To acquire the statuses and health statuses of all the avionic units (house-keeping data);
- To acquire experimental data from the In-Flight Measurement System for broadcasting to the TM/TC.

The **In-Flight Measurement System** is designed ad hoc for the specific needs of an experimental mission where the vehicle will not be recovered. Therefore, the data collected on-board represent the final goal of the activity for the purpose of design methodologies validation. Its main functions are:

- To acquire the experimental data/frames of:
  - Sensors (pressures, temperatures/heat fluxes, deformations, accelerations)
  - Actuator surfaces Cameras;
  - Propulsion and back-view Camera.
- Data level adaptation and conversion to the required levels;
- Data/Video mux and broadcasting directly to the TM/TC Units or through the FCC;
- To provide with physical links the Sensors and Video System.

Finally, the **Telemetry & Telecommands system** is in charge of:

- acquiring the experimental and housekeeping data from the FCC or IFMS and broadcasting to the GS via the Antennas system;
- acquiring Cameras compressed streams from the IFMS and broadcasting to the GS via Antennas system;
- receiving the Telecommand broadcasted by the Ground Segment (e.g. Flight Termination Command) and broadcast the to the Computer;
- implementing all the Transponder Functions (e.g. vehicle id and position transmission) required by the flight regulations and broadcast to ground.

3.3. Aerodynamics

The aerodynamic characterization conducted in this phase of the project has had the aim of assessing the aero-propulsive balance and the building of the aerodynamic database. Both activities have been performed by means of reacting and non-reacting CFD simulations.

3.3.1. Aero-propulsive Balance and Aerodynamic Efficiency

The verification of the aero-propulsive balance and aerodynamic efficiency in cruise conditions is conducted at two flight conditions (**Table 2**):

Table 2. Test Matrix for Hypersonic Cruise Conditions

Altitude	H = 27 km	H = 31.9 km
Static pressure p_∞	1828 Pa	875.5 Pa
Static temperature T_∞	222.3 K	235.97 K
Static density ρ_∞	0.02852 kg/m3	0.01293 kg/m3
Mach number M_∞	7.350	7.355
Flow velocity u_∞	2202 m/s	2264.7 m/s
MFR	**4.851 kg/s**	**2.246 kg/s**

Numerical CFD viscous simulations were carried out with the ANSYS FLUENT® CFD code on a grid composed of 7.6 million cells (Fig 10).

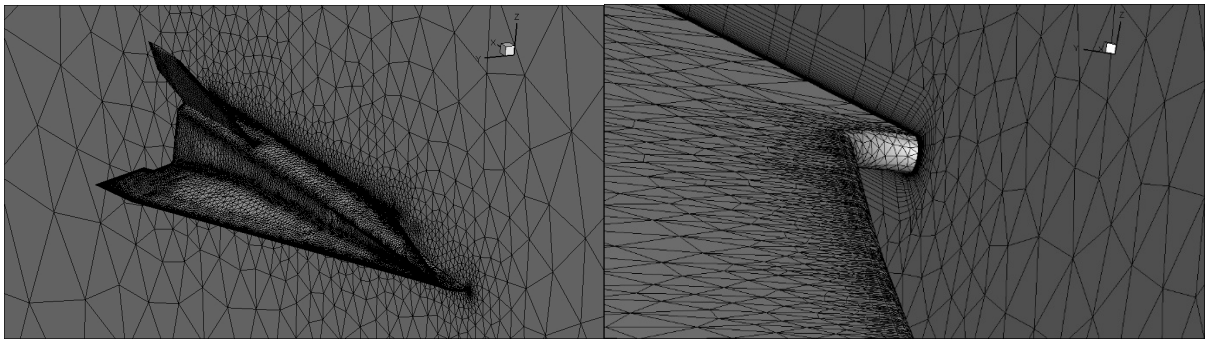

Fig 10: Computational grid for simulations with the engine on

Table 3 summarizes the aerodynamic parameters of interest. The values were extracted by distinguishing the external part (fuselage, wings and empennages) and the internal part composed of air intake, combustor and nozzle. The flight experiment takes place in motor-on conditions, and in these conditions, for the purposes of aerodynamic efficiency only, the external part of the aircraft is considered.
The results show that efficiency E_{ext} (external) is well above 4 (almost 5). In addition, total efficiency E_{tot}, which makes sense for the motor-off conditions that occur after the shutdown of the scramjet, is well within the mission requirements (value around 3.5).

Table 3: Summary of aerodynamic parameters of cruising with the engine off

H	Mach	Type	CL_ext	CL_int	CL_tot	CD_ext	CD_int	CD_tot	CM_ext	CM_int	CM_tot	E_ext	E_int	E_tot
27.00	7.350	No-Inj	0.04004	0.001299	0.041339	0.008267	0.00336	0.01163	-0.02362	-0.00304	-0.02667	4.8431	0.3865	3.5552
31.90	7.355	No-Inj	0.03996	0.001166	0.041130	0.008604	0.00345	0.01205	-0.02355	-0.00296	-0.0265	4.6449	0.3380	3.4125

For what concerns the aero-propulsive balance, it is necessary to verify that the thrust delivered by the scramjet engine is counterbalanced by the aerodynamic drag of the external part of the aircraft.
The net thrust, i.e. the gross thrust decreased by the drag of the air intake (which is considered to be part of the engine), must therefore be greater than, or equal to, the external drag.
Simulations with air-hydrogen reacting flow were therefore conducted under the same asymptotic conditions of Table 2. A single-step chemical scheme for modelling air-hydrogen combustion was used

that considers the only reaction between oxygen and hydrogen, with nitrogen that remains inert and unchanged along the entire internal duct.
Table 4 shows the main results in terms of axial forces for both motor-off and motor-on conditions. First of all, it can be noted that the aero-propulsive balance requirement is met at both altitudes. Indeed, the total force resistance (external + internal) is negative, which means that the thrust of the scramjet engine (Thrust > Drag) is higher than the external resistance.

Table 4: Summary of axial forces acting on the hypersonic propelled demonstrator

		Ext	Int	Tot
Forces (N)	**27 km**	**2820**	**-3032**	**-213**
Mot-on	**31.9 km**	**1357**	**-1380**	**-23**
Forces (N)	**27 km**	**2740**	**1113**	**3853**
Mot-off	**31.9 km**	**1367**	**548**	**1915**

3.3.2. Aerodynamic Database

The aerodynamic database is provided as a function of Mach number (M_∞), angle of attack (α) and the elevon deflections (δ_e) in *fuel-off* conditions. The reference quantities are reported in Table 5. The Centre of Gravity is located at x_{CoG}=2.33 m from the SHEV's nose.

Table 5: SHEV Reference Quantities

Reference Length (L_{ref})	4.1248 m
Reference Surface (S_{ref})	4.7936 m^2
Mass	1120 kg
x_{CoG} range	2.30÷2.33 m

The aerodynamic database of the SHEV vehicle has been completed from Mach 7.35 to Mach 2; indeed, the mission foresees, after the ignition time (at least 10 seconds at constant altitude), a gliding aerodynamically controlled phase followed by a splash down on the sea. The database will be then completed to cover the whole mission till splash down.
The CFD computations have been obtained running on the same grid of 7.6 million of cells and with the same turbulence model, but now in fuel-off conditions (see Table 6).
A sensitivity in fuel-on cruising conditions has been also performed by adding ±2deg to AoA=0 deg at M=7.35 while a range from -4° to +4° for the AoA in fuel-off ones has been considered. The fuel-off descent, based on the estimated preliminary trajectory, needs to be verified later by means of Flight-Mechanics analysis. The AEDB data will be released with increasing reliability for flight mechanics analysis and trajectory calculation in the framework of the project.

Looking at figures from Fig 11 to Fig 13 we can deduce that:

- there is a linear trend of CL for full vehicle (External + Internal), except in fuel-on conditions (M=7.35), where there is a decrease of the derivative CL_α with increasing of AoA;
- there is a quadratic trend of CD. At M=7.35 fuel-on conditions the aero-propulsive balance is "negative" at AoA=2° that means that the external drag is greater than the "net thrust" of the internal flow path. This is due to the fact that at higher angle of attack the intake is characterized by a certain airflow spillage and so the scramjet engine gives a lower "thrust". The opposite can be observed at AoA=-2° where there is a higher mass flow rate and thrust;
- in the gliding phase from M=7.35 to M=2 an out of trend of CL can be observed (see Fig 13). At M=3.5 the CL is lower than expected. This is due to the expulsion of the shock waves train from combustor duct, and the consequent positioning of the shock wave over the intake giving a local down-lift (i.e., the intake hysteresis phenomenon);
- the external coefficients are all regular as expected from linear aerodynamics. There is no influence of the shock wave train positioning along the gliding trajectory;

– from the internal coefficients it can be observed, as expected from previous considerations, great values of drag and down-lift at M=2 and 3.5 (expulsion of shock waves train), small values for other Mach numbers and, in particular, negative drag (that means positive internal thrust) at M=7.35 Fuel-On conditions.

Table 6: Test Matrix for CFD computations

h (km)	Mach	AoA	engine	P	Temp	Dens	a	Vel	mu
27.00	7.35	-2, 0, 2, 4	fuel-off/on	1847.46	223.65	0.028777	299.799	2203.52	1.47164E-05
26.19	7	-2, 0, 2, 4	fuel-off	2091.26	222.84	0.032693	299.255	2094.79	1.46711E-05
25.25	6	-2, 0, 2, 4	fuel-off	2416.16	221.90	0.037932	298.623	1791.74	1.46324E-05
23.36	5	-2, 0, 2, 4	fuel-off	3236.22	220.01	0.051243	297.349	1486.75	1.45123E-05
20.54	3.5	-2, 0, 2, 4	fuel-off	5028.52	217.19	0.080656	295.437	1034.03	1.43532E-05
17.72	2	-2, 0, 2, 4	fuel-off	7843.63	216.65	0.126124	295.070	590.14	1.43226E-05

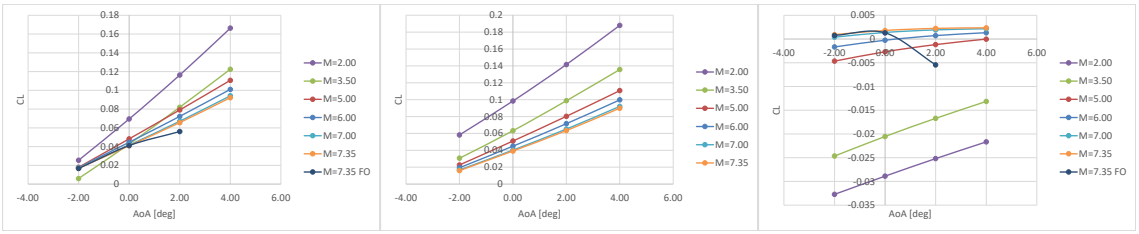

Fig 11: Lift Coefficient: Full vehicle, External part, Internal part

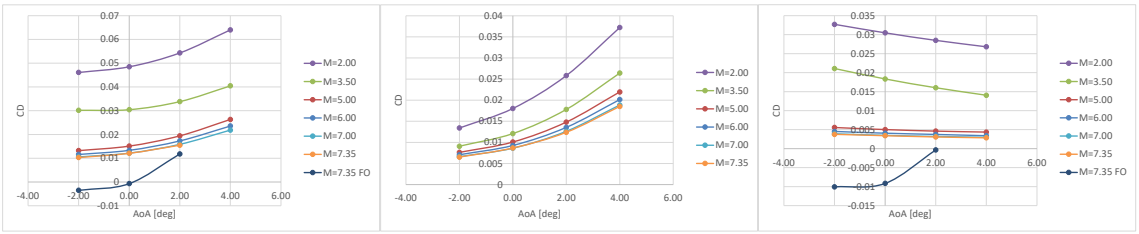

Fig 12: Drag Coefficient: Full vehicle, External part, Internal part

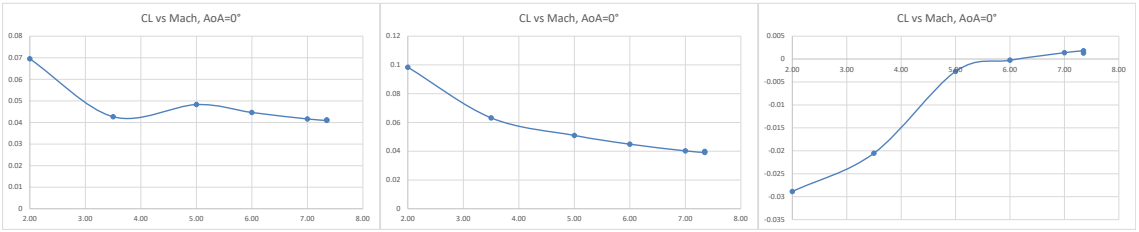

Fig 13: Lift Coefficient at AoA=0°: Full vehicle, External part, Internal part

The variation of the aerodynamic coefficients due to the control surfaces is assessed as the difference between the aerodynamic coefficients of the configuration evaluated with deflected elevon and the coefficients evaluated with the undeflected elevon (e.g., $\Delta C_M(\delta_e) = C_{M_{\delta_e}} - C_{M_{\delta_e=0}}$) on a simplified configuration composed by wing and elevon.

The following figures (Fig 14, Fig 15 and Fig 16) show, respectively, the lift, drag and pitching moment coefficient distributions in function of AoA for three different elevon deflections (-20°, -5°, +10°) and Mach numbers from 2 to 7.35. Please, note that the pitching moment is evaluated with respect to X_{CoG}=2.3099 m.

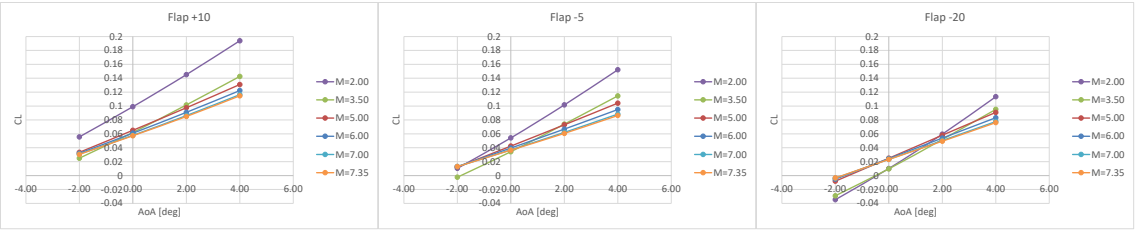

Fig 14: Lift Coefficient at three different elevon deflections

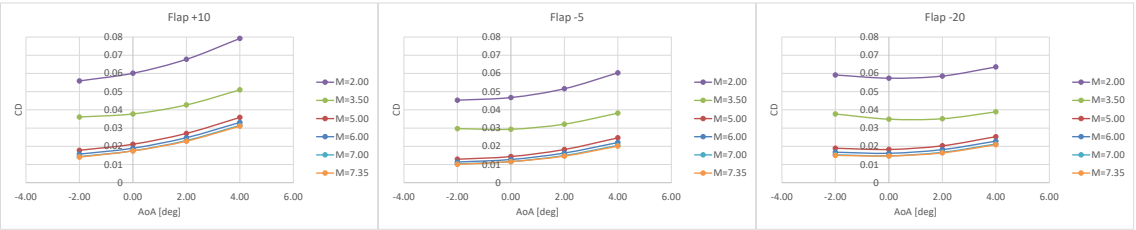

Fig 15: Drag Coefficient at three different elevon deflections

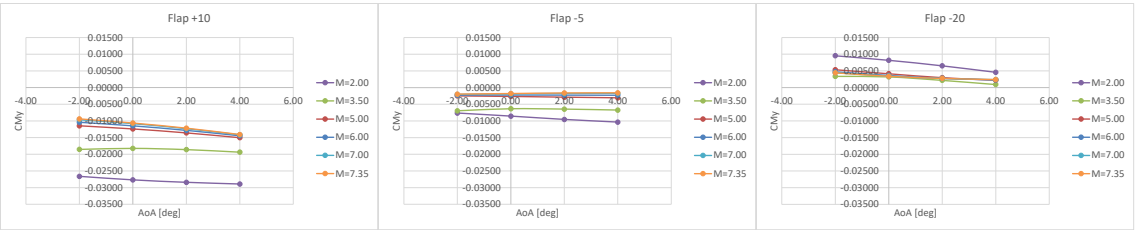

Fig 16: Pitching Moment Coefficient at three different elevon deflections

3.4. Flight Mechanics Analyses

The flight mechanics analyses of the Scramjet Hypersonic Experimental Vehicle have a twofold objective:

- To evaluate the demonstrator's flyability properties
- To define the nominal trajectory that fits the desired experimental mission profile.

The completion of both these tasks allows to check the feasibility of the SHEV mission and to compute the optimal position of the demonstrator's centre of gravity, supporting the definition of the vehicle configuration.

For a mission that is assumed purely longitudinal, the flyability analyses assess, in each point of the Mach number (M) – angle of attack (α) plane, the vehicle capability to achieve rotational trim in the longitudinal plane, to manoeuvre, and to be static stable in the trim points, that is, to satisfy the following properties:

$$\exists \delta_{Trim} \in [\delta_{min}, \delta_{max}] \; such \; that \; C_m(M, \alpha, \delta_{Trim}) = 0 \tag{1}$$

$$(1 - G_{man}) \cdot \delta_{min} \leq \delta_{Trim} \leq (1 - G_{man}) \cdot \delta_{max} \tag{2}$$

$$C_{m\alpha}(M, \alpha, \delta_{Trim}) < 0 \tag{3}$$

$$SM = -(C_{m\alpha}(M, \alpha, \delta_{Trim}) / C_{L\alpha}(M, \alpha, \delta_{Trim})) > 0 \tag{4}$$

where δ_{min} and δ_{max} indicate the minimum and maximum allowable deflection of the flap, respectively; G_{man} is the manoeuvrability margin, which varies between 0 and 1 (it is usually about 0.2) and quantifies the fraction of maximum flap deflection reserved to maneuver the aircraft with respect to the trim condition. The flyability properties of the vehicle depend on the position of its centre of gravity.

The nominal trajectory is computed by defining the guidance law, which for the considered mission coincides with the angle of attack profile. It is obtained solving the following nonlinear constrained optimization problem:

$$\min_{\alpha} J \quad such\ that \quad \begin{cases} \dot{x}(t) = F(\alpha(t), x(t), t) \\ B(\alpha(t), x(t), t) = 0 \\ C(\alpha(t), x(t), t) \leq 0 \\ \alpha_{min}(M) \leq \alpha(M) \leq \alpha_{max}(M) \end{cases} \tag{4}$$

The objective function J shall be properly defined. The constraint equations represent the dynamic equations of motion, the initial and final condition of the trajectory, the mission and system requirements, and the admissible range of variation for the angle of attack that guarantees good flyability properties. The selected objective function and the methodology applied to find a solution to the nonlinear constrained optimization problem are detailed described in [9].

A preliminary loop of the flight mechanics analyses has been performed. The analyses pointed out that the SHEV has satisfactory flyability properties if the CoG is placed along the longitudinal axis of the demonstrator and between 2243.9 and 2309.9 millimetres from the vehicle nose. At the forward limit of this range, if the motor is turned off, then the vehicle is trimmable with a satisfactory manoeuvrability margin almost everywhere, except for a small region at angle of attack bigger than 3 degrees and Mach number between 3 and 4.5; the flap deflection required to trim the demonstrator is always negative, as expected for this type of vehicle, and the static stability is guaranteed in the whole trimmable region. If the motor is on, then the vehicle is always trimmable and static stable; a satisfactory manoeuvrability margin is available for angle of attack lower than 1 degree, whereas the aerodynamic efficiency is bigger than 3 if the angle of attack is bigger than -0.55 degrees. For the CoG placed at the rearward limit of the identified allowable range, the vehicle is trimmable and manoeuvrable on the whole examined flight envelope, for both motor off and motor on. The flap deflection required to trim is still negative. If the motor is turned off, then there is a wide stability corridor in which the nominal trajectory can be placed. The stability margin for motor on values few percentage points if the angle of attack is negative, as typical for hypersonic vehicle. The aerodynamic efficiency is bigger than 3 for angle of attack bigger than -0.7 degrees.

The nominal trajectories have been computed for different positions of the CoG within the allowable range determined by the flyability analyses; one of them is shown in the following Fig 17. The obtained trajectories show similar characteristics and all their main parameters (aerodynamic efficiency, dynamic pressure, load factor, heat flux and load) are compliant with the preliminary thresholds defined at system level, confirming the feasibility of the mission [9].

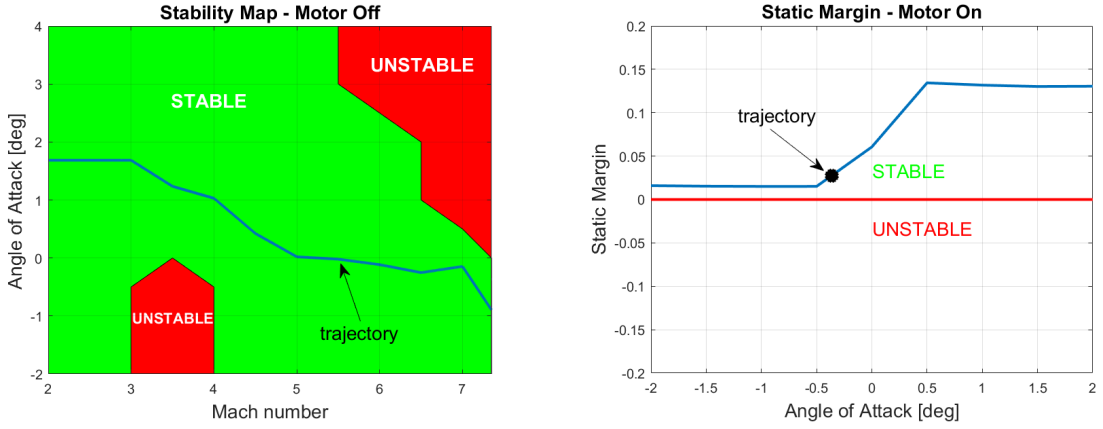

Fig 17. Nominal trajectory for rearward position of the CoG plotted on stability map for motor off (left) and on static margin for motor on (right)

4. Conclusions

This paper presents a summary of the main results achieved up today within the CIRA-ASI project on hypersonic flight, namely the CIRA "SPACE-IPERSONICA-TEC", funded by the national program PRORA, and the ASI-CIRA project "Research and Development of a hypersonic demonstrator", with the final goal of designing a hypersonic propelled demonstrator to increase the Technology Readiness Level of both system and technologies for future hypersonic transport vehicles.

First system activities, such as demonstrator configuration and mission scenario definition, aerodynamic database formulation, assessment of aero-propulsive balance, aerodynamic efficiency and preliminary nominal trajectory computation have been described in the paper.

The system PDR is foreseen in 2025.

Acknowledgements

The work has been co-funded by Italian Space Agency and CIRA ScPA in the frame of the agreement nr. 2022-13-HH.0-F43D22000410005.

References

1. Steelant, J. et al.: Conceptual Design of the High-Speed Propelled Experimental Flight Test Vehicle HEXAFLY. AIAA-2015-3539, 20th AIAA International Space Planes and Hypersonic Systems and Technologies Conference, Glasgow, Scotland, U.K. (2015).
2. Di Benedetto, S., Di Donato, M.P., Schettino, A., Scigliano, R., Nebula, F., Morani, G., Cristillo, D., Marini, M., Cardone, S., Steelant, J., Villace, V.: The high speed experimental flight test vehicle of HEXAFLY INT: a multidisciplinary design. CEAS Space Journal, DOI: 10.1007/s12567-020-00341-5, (2021).
3. J. Steelant, R. Varvill, C. Walton, S. Defoort, K. Hannemann, M. Marini: Achievements Obtained for Sustained Hypersonic Flight within the LAPCAT-II Project. AIAA-2015-3677, 20th AIAA International Space Planes and Hypersonic Systems and Technologies Conference, (2015).
4. Steelant, J., et al.: Achievements obtained within ATLLAS-II on Aero-Thermal Loaded Material Investigations for High-Speed Vehicles. 21st AIAA International Space Planes and Hypersonics Technologies Conference, China (2017).
5. Mack, A., Steelant, J., Adirim, H., Lentsch, A., Marini, M., Pilz, N.: FAST20XX: Achievements on European Suborbital Space Flight", 7th European Symposium on Aerothermodynamics, Brugge, Belgium, (2011).
6. Viola, N., Fusaro, R., Saracoglu, B., Schram, C., Grew,e V., Martinez, J., Marini, M., Hernandez, S., Lammers, K., Vincent, A., Hauglustaine, D., Liebhardt, B., Linke, F., Fureby, C.: Main Challenges and Goals of the H2020 STRATOFLY Project. Aerotecnica Missili & Spazio 100:95–110, https://doi.org/10.1007/s42496-021-00082-6, (2021).
7. Scigliano R., Marini M., Di Benedetto S., Albano M., Ranuzzi G.: Preliminary thermal assessment of an air-launched propelled hypersonic experimental vehicle. HiSST: 3rd International Conference on High-Speed Vehicle Science Technology, Busan, Korea, (2024).
8. Giuseppe C. Rufolo et al.: Space Rider Thermal Protection System, an enabling technology for reusable space transportation systems: design, development and qualification status. 74th International Astronautical Congress (IAC), Baku, Azerbaijan, (2023).
9. Vitale, A., Di Benedetto, S., Marini, M., Pizzurro, S., Bertacin, R.: Flyability Assessment and Trajectory Design for a Scramjet Hypersonic Experimental Vehicle. HiSST: 3rd International Conference on High-Speed Vehicle Science Technology, Busan, Korea, (2024).